

MR-Guided Vertebroplasty With Augmented Reality Image Overlay Navigation

Jan Fritz · Paweena U-Thainual · Tamas Ungi · Aaron J. Flammang ·
Sudhir Kathuria · Gabor Fichtinger · Iulian I. Iordachita · John A. Carrino

Received: 7 January 2014 / Accepted: 16 February 2014 / Published online: 11 April 2014

© Springer Science+Business Media New York and the Cardiovascular and Interventional Radiological Society of Europe (CIRSE) 2014

Abstract

Purpose To evaluate the feasibility of magnetic resonance imaging (MRI)-guided vertebroplasty at 1.5 Tesla using augmented reality image overlay navigation.

Materials and Methods Twenty-five unilateral vertebroplasties [5 of 25 (20 %) thoracic, 20 of 25 (80 %) lumbar] were prospectively planned in 5 human cadavers. A clinical 1.5-Tesla MRI system was used. An augmented reality image overlay navigation system and 3D Slicer visualization software were used for MRI display, planning, and needle navigation. Intermittent MRI was used to monitor placement of the MRI-compatible vertebroplasty needle. Cement injections (3 ml of polymethylmethacrylate) were performed outside the bore. The cement deposits were assessed on intermediate-weighted MR images. Outcome variables

included type of vertebral body access, number of required intermittent MRI control steps, location of final needle tip position, cement deposit location, and vertebroplasty time.

Results All planned procedures (25 of 25, 100 %) were performed. Sixteen of 25 (64 %) transpedicular and 9 of 25 (36 %) parapedicular access routes were used. Six (range 3–9) MRI control steps were required for needle placement. No inadvertent punctures were visualized. Final needle tip position and cement location were adequate in all cases (25 of 25, 100 %) with a target error of the final needle tip position of 6.1 ± 1.9 mm (range 0.3–8.7 mm) and a distance between the planned needle tip position and the center of the cement deposit of 4.3 mm (range 0.8–6.8 mm). Time requirement for one level was 16 (range 11–21) min.

Conclusion MRI-guided vertebroplasty using image overlay navigation is feasible allowing for accurate vertebral body access and cement deposition in cadaveric thoracic and lumbar vertebral bodies.

J. Fritz (✉) · S. Kathuria · J. A. Carrino
Russell H. Morgan Department of Radiology and Radiological
Science, Johns Hopkins University School of Medicine, 601
North Caroline Street, Baltimore, MD 21287, USA
e-mail: jfritz9@jhmi.edu

P. U-Thainual · I. I. Iordachita
Department of Mechanical Engineering and Laboratory for
Computational Sensing and Robotics, The Johns Hopkins
University, Baltimore, MD 21218, USA

P. U-Thainual · T. Ungi · G. Fichtinger
School of Computing, Queen's University, 557 Goodwin Hall,
Kingston, ON K7L 2N8, Canada

P. U-Thainual
Department of Mechanical and Materials Engineering, Queen's
University, McLaughlin Hall, Kingston, ON K7L 3N6, Canada

A. J. Flammang
Siemens Healthcare USA, Inc., 51 Valley Stream Pkwy,
Malvern, PA 19355, USA

Keywords Vertebroplasty · Interventional MR
imaging · MR imaging guidance · MR-guided

Introduction

Percutaneous vertebral cementoplasty (vertebroplasty) is used for pain palliation and structural stabilization [1–5] as the sole therapeutic procedure or in combination with vertebral body ablation techniques [6–10]. Fluoroscopy and computed tomography (CT) guidance techniques are commonly used [5, 11–13], but they result in variable radiation doses, which may lead to high exposure levels of ionizing radiation [11, 14, 15]. Furthermore, the low soft-tissue contrast resolution of both techniques may limit the conspicuity of anatomic structures and vertebral body lesions with little or no osseous destruction.

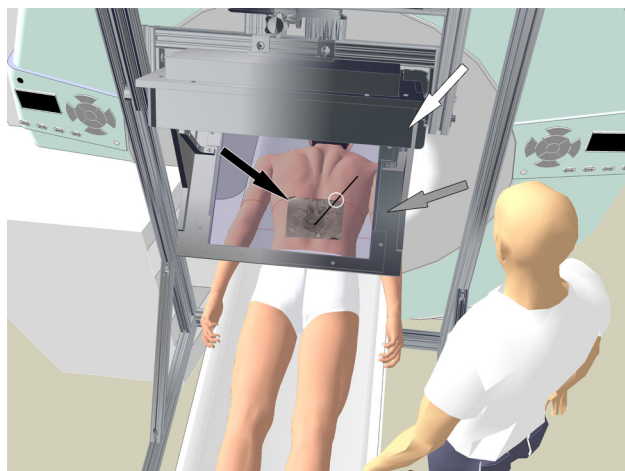


Fig. 1 Interventional setup with image overlay navigation system. Computer-aided design shows a clinical 1.5-Tesla MRI system and the stand-alone augmented reality image overlay navigation system consisting of a free-standing frame and an LCD display (*white arrow*) used for passive projection of the MR images on the semitransparent mirror (*gray arrow*), which reflects the image back into the operator's line of sight. This creates apparent hybrid views of the projected MR image (*black arrow*) and the subject that appear fused. The *black line* indicates a transpedicular virtual needle path. The *white circle* symbols the skin entry site formed by the intersection of the laser line (*red*) and the projected virtual needle path (Color figure online)

As potential alternative guidance technique, interventional magnetic resonance imaging (MRI) imaging offers favorable attributes for vertebroplasty, such as no ionizing radiation, true multiplanar cross-sectional imaging, and unparalleled contrast resolution [16–21]. MRI guidance has also the potential to facilitate temperature mapping of concomitant thermal vertebral body ablation [22, 23].

Successful MRI-guided vertebroplasty require accurate targeting and needle placement, which are challenging because of limited space inside the bore of widely available 1.5-Tesla MRI systems. Augmented reality navigation employing image overlay technology may solve this problem by providing navigation outside the bore [24]. Therefore, the purpose of this study was to prospectively evaluate the feasibility MRI-guided vertebroplasty using augmented reality image overlay navigation in human cadavers.

Materials and Methods

System Description

A commercially available 1.5-Tesla MRI system (MAGNETOM Espree; Siemens Healthcare, Erlangen, Germany), a MRI-compatible augmented reality image overlay navigation system (Fig. 1) [25], and 10 cm-long, 11G MRI-compatible vertebroplasty needle (Somatex, Teltow, Germany) were used. 3D Slicer (The Brigham and Women's

Hospital, Inc., Boston, MA, USA) open-source medical image analysis and visualization software (<http://www.slicer.org>) and the loadable module PerkStation (Queen's University, Kingston, ON, Canada) were used for display of MR images, identification of targets, planning of virtual needle paths, and needle navigation [26, 27] (Fig. 2A).

The navigation system provided MRI guidance through the projection of combined axial MR images and operator-defined virtual needle paths, which created an apparent fusion of the projected axial MR images and the patient under the system [28]. Needle placement consisted of alternating steps of image overlay navigated needle advancement outside the bore and under the navigation system as well as MRI control with the patient inside the bore. The automatic table function was used to translate the subject from the bore of the MRI system under the navigation system in appropriate location to match the projected MR image with the predefined target location and vice versa. The needle was placed by maneuvering the needle along the virtual needle path (Figs. 1, 2B).

Specimen

Five nonembalmed, full spine torso human cadavers (four men and one woman; age range at death range 65–82 years; mean age at death 73 years) were used. Two of five (40 %) cadavers were of small size [16–18.5 kg/m² living body mass index (BMI)]; 2 of 5 (40 %) were of medium size (18.5–25 kg/m² BMI), and 1 of 5 (20 %) was of large size (25–30 kg/m² BMI) [29]. All subjects were obtained and handled in accordance with our institutional rules and in accordance with the Health Insurance Portability and Accountability Act. The frozen cadaveric subjects were allowed to thaw for 24 h at room temperature (~20–22 °C) before MRI.

Research Plan

A total of 25 unilateral vertebroplasties were prospectively planned, including 5 of 25 (20 %) thoracic and 20 of 25 (80 %) lumbar vertebroplasty (Fig. 2). In each subject, 5 vertebroplasties were attempted. The study was performed on 5 different days (one subject per day) over a time period of 6 weeks. Procedures were performed by a single operator with 10 years of experience in percutaneous musculoskeletal procedures and interventional MRI. Initial experience and training was accomplished before the study with image overlay navigated puncture of 5 vertebral bodies of a cadaveric lumbar spine specimen.

Because the presence of vertebral body fractures in the obtained specimens was unknown, each procedure started with MRI of the entire thoracic and lumbar spine using an isotropic, T2-weighted MRI pulse sequence (three-

dimensional Sampling Perfection with Application optimized Contrasts using different flip angle Evolutions [SPACE]) with the following parameters: repetition time (TR) 1,400 ms; echo time (TE) 100 ms; flip angle (FA) 120°; averages (Av) 2; echo train length (ETL) 117; voxel size 1 × 1 × 1 mm; field of view (FOV) 192 × 168 mm; base resolution (BR) 192 pixel; phase resolution (PR) 100 %; and bandwidth (BW) 744 Hz. If present, vertebral bodies with compression deformities were selected (Fig. 2). Otherwise, vertebral bodies were selected randomly according to a computer algorithm.

Workflow

All cadavers were placed prone on the table of the MRI system. Parallel MRI was employed using table coil elements and a flexible loop-shaped radiofrequency surface receiver coil (Siemens Healthcare) with a diameter of 19 cm, which was freely movable and centered over the target site.

The initially acquired high-resolution 3D SPACE MRI data set was loaded into 3D Slicer software for planning and navigation. The operator determined the most suitable access to the previously defined vertebral body, prescribed the virtual needle path, and defined the final needle tip position facilitated through simultaneous display of axial, sagittal, and coronal reformats of the isotropic MRI data set by the PerkStation module in 3D Slicer (Fig. 2A). Depending on the individual anatomy, a transpedicular or parapedicular access was chosen.

For each vertebroplasty target, the projected MR image contained the virtual needle path with calculated insertion depth (Fig. 2B). The automatic table of the MRI system was moved under the navigation system in appropriate location. The skin entry point was chosen as indicated by the virtual intersection of the laser of the overlay system and the displayed virtual needle path (Fig. 2B). If necessary, the surface coil was shifted to include the skin entry site centrally. The surface loop coil was fixed with tape and stayed in place for the entire procedure, which facilitated intermittent MRI acquisition for monitoring of the needle placement, which was similar to previously described techniques in patients [16, 20, 30].

An appropriate skin incision was created to allow introduction of the needle. The operator maneuvered the MRI-compatible vertebroplasty needle along the displayed virtual needle path into the defined entry site of the vertebral body (Fig. 2B), and the cortex was penetrated using an MRI-compatible hammer. Using intermittent MRI control of the needle position (axial turbo spin echo MR sequence TR/TE 1800/60, FA 100, Av 1, ETL 14, slice thickness 3 mm, number of slices 7, FOV 349 × 209 mm, BR 320 pixels, PR

58 %, BW 388 Hz, and acquisition time 34 s), the needle was advanced step-wise to the target point.

Once the final needle position was confirmed, 3 ml of polymethylmethacrylate cement (Somatex, Teltow, Germany) was injected while the cadaveric specimen was outside the bore. Finally, 3D SPACE MR images (sequence parameters as previously described) of the treated level were acquired.

Assessment of Outcome Variables

The type of vertebral body access was categorized into transpedicular versus parapedicular.

The number of intermittent MRI control steps required for needle placement was defined as pairs of needle advancement, and MRI control was assessed.

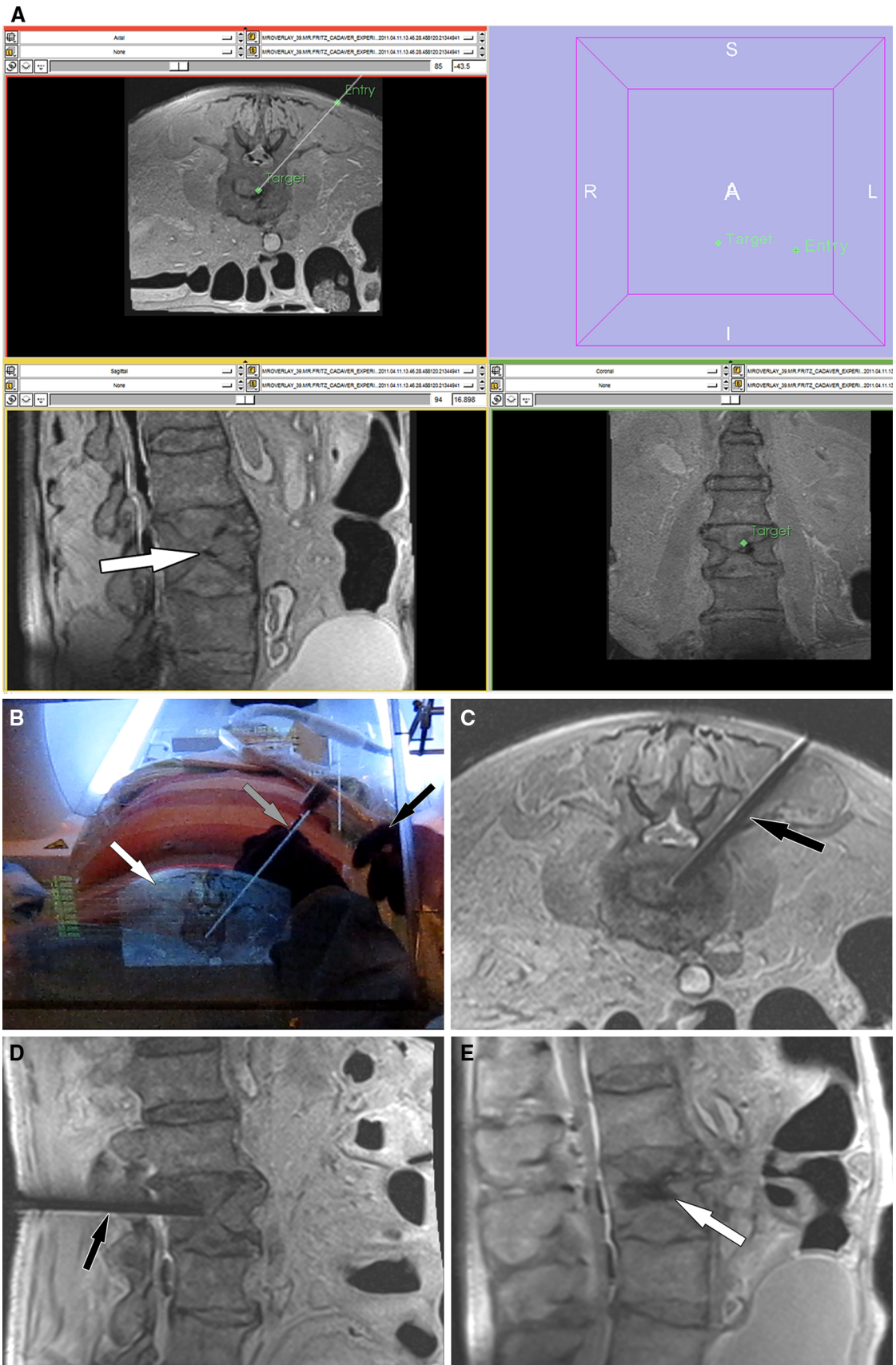
The target error of the needle tip, defined as the Euclidean distance between the planned and final position of the tip of the needle, was assessed. PerkStation was used for calculations by comparing the planned location of the needle tip with the location of the needle tip as manually determined on the final axial turbo spin echo MR images used for needle control [27]. Measurements were performed three times. The median was used.

The intravertebral cement location was assessed by measuring the Euclidean distance between the planned needle tip position and the geometric axial plane center of the cement deposit, which was defined as the intersection of the longest axial and shortest axial diameter. Measurements were carried in similar fashion as for the target error of the needle tip using PerkStation [31]. Measurements were performed three times. The median was used. The presence of extravertebral cement spread was recorded as well.

The length of time for vertebroplasty of a single level—including planning, operator calibration, needle placement and intermittent MRI control, cement injection, and acquisition of the final 3D SPACE MR images of the treated level—was calculated from the time information of the DICOM headers.

Statistical and Quantitative Assessments

Statistical analysis was performed using statistical software (JMP, version 7.01; SAS Institute Cary, NC). Categorical variables were expressed as frequencies and proportions. Quantitative variables were expressed as median with minimum and maximum values. Intrarater variability was expressed by use of the coefficient of variation (CV) as $CV = \sigma/\mu$, where σ is the first SD, and μ is the arithmetic mean. A p value of <0.05 was considered to indicate a significant difference.



◀**Fig. 2** Transpedicular MR-guided lumbar vertebroplasty with augmented reality image overlay navigation. **A** PerkStation interface shows endplate compression deformity of the L3 vertebral body (*white arrow*) and the planned needle path (*line*) with target point and skin entry point. **B** Intraoperative photograph of the operator view shows the hybrid view of the subject and projected MR image (*white arrow*), transpedicular virtual needle path (*gray arrow*) with superimposed vertebroplasty needle, and the operator's hand (*black arrow*) holding an MRI-compatible hammer. Axial **C** and sagittal **D** T2-weighted turbo spin echo MR image after needle placement shows the tip of the needle (*black arrows*) at the target. **E** Sagittal T2-weighted 3D turbo spin echo (SPACE) MR image after injection of 3 ml of polymethylmethacrylate cement shows the hypointense cement deposit centrally (*white arrow*) (Color figure online)

Results

All planned procedures (25 of 25, 100 %) were performed, including 5 of 25 thoracic vertebroplasties and 20 of 25 lumbar vertebroplasties (Fig. 2). Of those, 16 of 25 (64 %) were performed with a transpedicular access (Fig. 2) and 9 of 25 (36 %) with a parapedicular access route. Procedures were feasible in all three cadaver sizes. For the large cadaver, the height of the navigation system was individually adjusted to create a sufficient amount of space for access and contact-free handling. A median average of 6 (range 3–9) MRI control were required to place a needle into the targeted vertebral body. The target error of the final needle tip position was 6.1 ± 1.9 mm (range 0.3–8.7; CV = 11.2 ± 7.9 %; range 6.7–14.8 %). The distance between the planned needle tip position and the center of the cement deposit was 4.3 mm (range 0.8–6.8). The center of all cement deposits was located inside the targeted vertebral body (Fig. 2E). There was no extravertebral cement leakage, including no leakage into the central spinal canal or neural foramina. The median length of time for one vertebroplasty level was 16 min (range 11–21).

Discussion

The results of our study show that MRI-guided vertebroplasty is feasible to allow for sufficiently accurate transpedicular and parapedicular vertebral body access and intravertebral cement delivery. Image overlay navigation was useful for the assessment of anatomy, determination of vertebral body access, and guidance of needle placement. An optimized turbo spin echo pulse sequence is capable of creating a well-defined artifact of an MRI-compatible vertebroplasty needle for accurate localization of the needle tip and to avoid obscuring critical anatomic structures, such as vertebral body cortex, thecal sac, and spinal nerves. Intermediate-weighted MRI creates a high contrast-to-noise ratio between the hypointense cement and the hyperintense vertebral body bone marrow signal, thus

making the cement deposit inside the vertebral body well visible.

Interventional MRI has evolved into clinically beneficial and practically useful musculoskeletal procedures and techniques [16–19, 32–43]. Although placement of spinal needles inside a bore of a magnet is feasible, the spatial limitations and distance to the isocenter, even inside wide-bore MRI systems [44], likely prevents accurate and sterile advancement of a vertebroplasty needle inside the vertebral body because two hands are needed at the skin entry site, one to hold the needle and one for the hammer [45]. Assisted real-time MRI guidance could be helpful for the determination of the skin entry site and needle advancement in the soft tissues dorsal to the vertebral body inside the bore [46]. Vertebral body puncture could occur outside with indirect free-hand navigation by a separate in-room monitor [47]; however, the visual separation of target and image information may complicate this task. Image-overlay navigation facilitated accurate vertebral body puncture outside the bore by providing virtual reality MRI guidance through the simultaneous visualization of the MR images and the vertebral body target.

We used axial images for navigation, although the actual needle paths for transpedicular access was often oblique in craniocaudally direction. This was not found to limit the operator's ability of successful puncture because once the needle penetrated the cortex at the defined target point in correct alignment with the displayed virtual path, the needle advancement performed in a stepwise, rotating fashion was guided by the pedicle cortex and was safely achieved in all cases as confirmed by axial and sagittal, intermittent MRI control. The addition of nonaxial image navigation capabilities would be expected to improve the versatility of this navigation technology.

Cement visibility is important for the characterization of cement spread and extravertebral leakage [5, 48]. The use of intermediate echo time pulse sequences resulted in high contrast conspicuity between the hypointense injected cement and the hyperintense vertebral body tissues. However, because of flow-related void of signal in vessels with fast spin echo technique, intravascular uptake of hypointense-appearing cement may not have been detectable in our study [48]. More recently described cement with T1-shortening capabilities appears hyperintense on T1-weighted images [49], which can be beneficial for the visualization of cement spread into hypointense tissues and structures, thus potentially rendering intravascular uptake detectable.

A limitation of MRI-guided vertebroplasty may be the difficulty of real-time imaging monitoring of cement injections. For the purpose of this initial investigation, cement injections were not monitored real-time but were performed outside the MRI system. Similar to our current

practice of CT-guided vertebroplasty, however, intermittent MRI monitoring after every 0.5 ml of injected cement can be employed as an alternative approach for potentially early detection of extravertebral spread.

Spinal neoplasms may be treated with a combination of percutaneous ablation of the vertebral body lesion and subsequent cement augmentation [6–8, 10]. MRI-guided ablation of vertebral body lesions has been shown to be feasible [50] and may be advantageous because of high lesion conspicuity and temperature-monitoring capabilities of the ablation zone and surrounding susceptible structures [22, 23]. With the described technique, the combination of MRI-guided vertebral body ablation and cement augmentation of the ablation zone seems possible.

Our study had limitations. First, because we used cadaveric specimens, patient motion and respiration were not present, which may influence the performance of static image-overlay navigation. However, vertebroplasty is often performed with the patient under general anesthesia with controlled respiration and limited motion. Second, because the presence and location of vertebral body compression deformities was unknown, the MRI data set, which was later used for planning, covered the entire thoracolumbar spine. The given vertebroplasty time therefore did not include the acquisition time of a dedicated MRI data set of the respective vertebral body level, which is approximately 3 min. Third, because the presence of vertebral body lesions and compression fractures of cadavers was not known, the sample size only included two vertebral body compression fractures, whereas the remainder of vertebroplasties were performed in normal-appearing vertebral bodies. Fourth, although high-resolution, intermediate-weighted MR images visualized the intravertebral cement well, subtle cement leakage may have gone undetected. This could be assessed with CT correlation in a future study.

Based on the results of this human cadaver study, we conclude that MRI-guided vertebroplasty with image-overlay navigation is feasible with sufficient accuracy for cement augmentation of thoracic and lumbar vertebral bodies. We believe that MRI-guided vertebroplasty could be a beneficial technique in a properly selected group of patients as well as a supplement to CT and fluoroscopy as the principal imaging-guidance techniques, thus warranting further investigation.

Acknowledgments National Cancer Institute, 1 R01 CA118371-01A2-Image Overlay for MRI-Guided Needle Insertions. Cancer Care Ontario Research Chair in Cancer Imaging (Gabor Fichtinger). NSERC CREATE in Human Mobility (Paweena U-Thainual). Ontario Ministry of Innovation postdoctoral fellowship (Tamas Ungi). Somatex Medical Technologies GmbH, Teltow, Germany, supported this study by providing the MRI-compatible vertebroplasty needles and cement.

Conflict of interest Jan Fritz, Paweena U-Thainual, Tamas Ungi, Aaron J. Flammang, Sudhir Kathuria, Gabor Fichtinger, Iulian I. Iordachita, and John A. Carrino received grants from the National Cancer Institute, 1 R01 CA118371-01A2-Image Overlay for MRI-Guided Needle Insertions, as well as nonfinancial support from Somatex Medical Technologies GmbH, Teltow, Germany, during the conduct of the study. Jan Fritz, Gabor Fichtinger, and Sudhir Kathuria received grants and nonfinancial support from Siemens AG outside the submitted work. Paweena U-Thainual received grants from NSERC CREATE in Human Mobility during the conduct of the study. Tamas Ungi received grants and personal fees from Ontario Ministry of Innovation postdoctoral fellowship during the conduct of the study. Gabor Fichtinger received grants from Cancer Care Ontario Research Chair in Cancer Imaging during the conduct of the study. John Carrino received grants from Toshiba and Carestream, as well as personal fees from General Electric, Siemens, and BioClinica, outside the submitted work.

References

1. Anselmetti GC, Manca A, Montemurro F et al (2012) Percutaneous vertebroplasty in multiple myeloma: prospective long-term follow-up in 106 consecutive patients. *Cardiovasc Intervent Radiol* 35(1):139–145
2. Masala S, Pipitone V, Tomassini M, Massari F, Romagnoli A, Simonetti G (2006) Percutaneous vertebroplasty in painful Schmorl nodes. *Cardiovasc Intervent Radiol* 29(1):97–101
3. Anselmetti GC, Corrao G, Monica PD et al (2007) Pain relief following percutaneous vertebroplasty: results of a series of 283 consecutive patients treated in a single institution. *Cardiovasc Intervent Radiol* 30(3):441–447
4. Gangi A, Clark WA (2010) Have recent vertebroplasty trials changed the indications for vertebroplasty? *Cardiovasc Intervent Radiol* 33(4):677–680
5. Gangi A, Sabharwal T, Irani FG, Buy X, Morales JP, Adam A (2006) Quality assurance guidelines for percutaneous vertebroplasty. *Cardiovasc Intervent Radiol* 29(2):173–178
6. Orgera G, Krokidis M, Matteoli M et al (2013) Percutaneous vertebroplasty for pain management in patients with multiple myeloma: is radiofrequency ablation necessary? *Cardiovasc Intervent Radiol* 37(1):203–210
7. Gronemeyer DH, Schirp S, Gevargez A (2002) Image-guided radiofrequency ablation of spinal tumors: preliminary experience with an expandable array electrode. *Cancer J* 8(1):33–39
8. Schaefer O, Lohrmann C, Markmiller M, Uhrmeister P, Langer M (2003) Technical innovation. Combined treatment of a spinal metastasis with radiofrequency heat ablation and vertebroplasty. *AJR Am J Roentgenol* 180(4):1075–1077
9. Kelekis A, Filippiadis DK, Martin JB, Kelekis NL (2013) Aggressive vertebral hemangioma treated with combination of vertebroplasty and sclerotherapy through transpedicular and direct approach. *Cardiovasc Intervent Radiol* [Epub ahead of print]
10. Masala S, Roselli M, Manenti G, Mammucari M, Bartolucci DA, Simonetti G (2008) Percutaneous cryoablation and vertebroplasty: a case report. *Cardiovasc Intervent Radiol* 31(3):669–672
11. Amoretti N, Lesbats V, Marcy PY et al (2010) Dual guidance (CT and fluoroscopy) vertebroplasty: radiation dose to radiologists. How much and where? *Skeletal Radiol* 39(12):1229–1235
12. Braak SJ, Zuurmond K, Aerts HC et al (2013) Feasibility study of needle placement in percutaneous vertebroplasty: cone-beam computed tomography guidance versus conventional fluoroscopy. *Cardiovasc Intervent Radiol* 36(4):1120–1126

13. Gangi A, Kastler BA, Dietemann JL (1994) Percutaneous vertebroplasty guided by a combination of CT and fluoroscopy. *AJNR Am J Neuroradiol* 15(1):83–86
14. Perisinakis K, Damilakis J, Theocharopoulos N, Papadokostakis G, Hadjipavlou A, Gourtsoyiannis N (2004) Patient exposure and associated radiation risks from fluoroscopically guided vertebroplasty or kyphoplasty. *Radiology* 232(3):701–707
15. Joemai RM, Zweers D, Obermann WR, Geleijns J (2009) Assessment of patient and occupational dose in established and new applications of MDCT fluoroscopy. *AJR Am J Roentgenol* 192(4):881–886
16. Fritz J, Tzaribachev N, Thomas C et al (2012) Magnetic resonance imaging-guided osseous biopsy in children with chronic recurrent multifocal osteomyelitis. *Cardiovasc Intervent Radiol* 35(1):146–153
17. Maurer MH, Disch AC, Hartwig T, et al (2013) Outcome study of real-time MR-guided cervical periradicular injection therapy in an open 1.0 Tesla MRI system. *Cardiovasc Intervent Radiol* [Epub ahead of print]
18. Streitparth F, Gebauer B, Melcher I et al (2009) MR-guided laser ablation of osteoid osteoma in an open high-field system (1.0 T). *Cardiovasc Intervent Radiol* 32(2):320–325
19. Akural E, Ojala RO, Jarvimaki V, Kariniemi J, Tervonen OA, Blanco SR (2013) MR-guided neurolytic celiac plexus ablation: an evaluation of effect and injection spread pattern in cancer patients with celiac tumor infiltration. *Cardiovasc Intervent Radiol* 36(2):472–478
20. Fritz J, Henes JC, Thomas C et al (2008) Diagnostic and interventional MRI of the sacroiliac joints using a 1.5-T open-bore magnet: a one-stop-shopping approach. *AJR Am J Roentgenol* 191(6):1717–1724
21. Fritz J, Thomas C, Tzaribachev N et al (2009) MRI-guided injection procedures of the temporomandibular joints in children and adults: technique, accuracy, and safety. *AJR Am J Roentgenol* 193(4):1148–1154
22. Binkert CA, Nanz D, Bootz F et al (2002) Laser-induced thermotherapy of the vertebral body: preliminary assessment of safety and real-time magnetic resonance monitoring in an animal model. *Invest Radiol* 37(10):557–561
23. Streitparth F, Walter T, Wonneberger U, et al. (2013) MR guidance and thermometry of percutaneous laser disc decompression in open MRI: An ex vivo study. *Cardiovasc Intervent Radiol* [Epub ahead of print]
24. Fritz J, Thainual P, Ungi T et al (2013) Augmented reality visualization using image overlay technology for MR-guided interventions: cadaveric bone biopsy at 1.5 T. *Invest Radiol* 48(6):464–470
25. U-Thainual P, Fritz J, Moonjaita C et al (2012) MR image overlay guidance: system evaluation for preclinical use. *Int J Comput Assist Radiol Surg* 8(3):365–378
26. Kikinis R, Pieper S (2011) 3D Slicer as a tool for interactive brain tumor segmentation. *Conf Proc IEEE Eng Med Biol Soc* 1:6982–6984
27. Vikal S, Thainual P, Carrino JA, Iordachita I, Fischer GS, Fichtinger G (2010) Perk Station—Percutaneous surgery training and performance measurement platform. *Comput Med Imaging Graph* 34(1):19–32
28. Fritz J, Thainual P, Ungi T et al (2012) Augmented reality visualization with use of image overlay technology for MR imaging-guided interventions: assessment of performance in cadaveric shoulder and hip arthrography at 1.5 T. *Radiology* 265(1):254–259
29. Obesity: preventing and managing the global epidemic Report of a WHO consultation (2000) *World Health Organ Tech Rep Ser* 894(i–xii):1–253
30. Streitparth F, Walter T, Wonneberger U et al (2010) Image-guided spinal injection procedures in open high-field MRI with vertical field orientation: feasibility and technical features. *Eur Radiol* 20(2):395–403
31. Fritz J, Thainual P, Ungi T et al (2012) Augmented reality visualisation using an image overlay system for MR-guided interventions: technical performance of spine injection procedures in human cadavers at 1.5 Tesla. *Eur Radiol* 23(1):235–245
32. Blanco SR, Klemola R, Ojala R et al (2002) MRI-guided trephine biopsy and fine-needle aspiration in the diagnosis of bone lesions in low-field (0.23 T) MRI system using optical instrument tracking. *Eur Radiol* 12(4):830–835
33. Blanco SR, Carrino JA (2005) Musculoskeletal interventional MR imaging. *Magn Reson Imaging Clin North Am* 13(3):519–532
34. Carrino JA, Blanco R (2006) Magnetic resonance-guided musculoskeletal interventional radiology. *Semin Musculoskelet Radiol* 10(2):159–174
35. Carrino JA, Khurana B, Ready JE, Silverman SG, Winalski CS (2007) Magnetic resonance imaging-guided percutaneous biopsy of musculoskeletal lesions. *J Bone Joint Surg Am* 89(10):2179–2187
36. Genant JW, Vandevenne JE, Bergman AG et al (2002) Interventional musculoskeletal procedures performed by using MR imaging guidance with a vertically open MR unit: assessment of techniques and applicability. *Radiology* 223(1):127–136
37. Koenig CW, Duda SH, Truebenbach J et al (2001) MR-guided biopsy of musculoskeletal lesions in a low-field system. *J Magn Reson Imaging* 13(5):761–768
38. Lewin JS, Petersilge CA, Hatem SF et al (1998) Interactive MR imaging-guided biopsy and aspiration with a modified clinical C-arm system. *AJR Am J Roentgenol* 170(6):1593–1601
39. Ojala R, Sequeiros RB, Klemola R, Vahala E, Jyrkinen L, Tervonen O (2002) MR-guided bone biopsy: preliminary report of a new guiding method. *J Magn Reson Imaging* 15(1):82–86
40. Parkkola RK, Mattila KT, Heikkila JT et al (2001) Dynamic contrast-enhanced MR imaging and MR-guided bone biopsy on a 0.23 T open imager. *Skeletal Radiol* 30(11):620–624
41. Smith KA, Carrino J (2008) MRI-guided interventions of the musculoskeletal system. *J Magn Reson Imaging* 27(2):339–346
42. Weiss CR, Nour SG, Lewin JS (2008) MR-guided biopsy: a review of current techniques and applications. *J Magn Reson Imaging* 27(2):311–325
43. Kerimaa P, Marttila A, Hyvonen P et al (2013) MRI-guided biopsy and fine needle aspiration biopsy (FNAB) in the diagnosis of musculoskeletal lesions. *Eur J Radiol* 82(12):2328–2333
44. Fritz J, Thomas C, Clasen S, Claussen CD, Lewin JS, Pereira PL (2009) Freehand real-time MRI-guided lumbar spinal injection procedures at 1.5 T: feasibility, accuracy, and safety. *AJR Am J Roentgenol* 192(4):W161–W167
45. Seimenis I, Tsekos NV, Keroglou C, Eracleous E, Pitris C, Christoforou EG (2012) An approach for preoperative planning and performance of MR-guided interventions demonstrated with a manual manipulator in a 1.5 T MRI scanner. *Cardiovasc Intervent Radiol* 35(2):359–367
46. Rothgang E, Gilson WD, Wacker F, Hornegger J, Lorenz CH, Weiss CR (2013) Rapid freehand MR-guided percutaneous needle interventions: an image-based approach to improve workflow and feasibility. *J Magn Reson Imaging* 37(5):1202–1212
47. Fritz J, Thainual P, Ungi T et al (2012) Augmented reality visualization with image overlay for MRI-guided intervention: accuracy for lumbar spinal procedures with a 1.5-T MRI system. *AJR Am J Roentgenol* 198(3):W266–W273
48. Baumann C, Fuchs H, Kiwit J, Westphalen K, Hierholzer J (2007) Complications in percutaneous vertebroplasty associated

- with puncture or cement leakage. *Cardiovasc Intervent Radiol* 30(2):161–168
49. Wichlas F, Seebauer CJ, Schilling R et al (2012) A signal-inducing bone cement for magnetic resonance imaging-guided spinal surgery based on hydroxyapatite and polymethylmethacrylate. *Cardiovasc Intervent Radiol* 35(3):661–667
50. Nour SG, Aschoff AJ, Mitchell IC, Emancipator SN, Duerk JL, Lewin JS (2002) MR imaging-guided radio-frequency thermal ablation of the lumbar vertebrae in porcine models. *Radiology* 224(2):452–462